INTERNATIONAL JOURNAL FOR NUMERICAL METHODS IN FLUIDS
Int. J. Numer. Meth. Fluids 2010; **62**:291–312
Published online 3 March 2009 in Wiley InterScience (www.interscience.wiley.com). DOI: 10.1002/fld.2022

Hybrid modelling for simulation of scour and flow patterns in laboratory flumes

Aytac Guven*, †, ‡ and Mustafa Gunal

Department of Civil Engineering, University of Gaziantep, 27310 Gaizantep, Turkey

SUMMARY

In this study, a hybrid numerical–mathematical model is developed, which simulates the temporal evolution of local scour and flow patterns in laboratory flumes. The mathematical module calculates the shape of the scour hole by solving an integro-parabolic equation. The numerical module simulates the two-dimensional laterally averaged flow patterns in the corresponding scour hole. The hybrid model is verified by experimental data taken from the literature. The hybrid model predicted the temporal evolution of local scour and simulated the flow patterns in and around the scoured zone in good agreement with the experimental ones. The proposed hybrid model proved to be efficient when used in complex local scour and turbulent flow problems. Copyright © 2009 John Wiley & Sons, Ltd.

Received 3 December 2008; Revised 27 January 2009; Accepted 28 January 2009

KEY WORDS: scour; turbulent jet; numerical modelling; mathematical modelling; flume; turbulence

1. INTRODUCTION

Prediction and control of scouring are important considerations in the safe design of hydraulic structures, for example, near cooling pools of power plants, around bridge piers, in spillway and culvert outlets and in irrigation channels. Large-scale erosion caused by fluid flow to hydraulic structures is of obvious concern because the foundations can be undermined leading to structural failure [1].

In recent years, with the ever-increasing capabilities of computer hardware and software, and due to the time-consuming and expensive nature of experimental research on scouring processes caused

*Correspondence to: Aytac Guven, Department of Civil Engineering, University of Gaziantep, 27310 Gaizantep, Turkey.
†E-mail: aguven@gantep.edu.tr
‡Assistant Professor.

Contract/grant sponsor: Scientific Research Projects Governing Unit of Gaziantep University

by flowing water, several researchers have focused on numerical simulation of the interaction of the fluid flow and the movable bed [2].

Early studies on numerical modelling of local scour go back to the mid 1970s. Zaghloul and McCorquodale [3] proposed a numerical model that predicted the depth and shape of the local scour hole using the Helmholtz–Poisson form of the Reynolds equations with constant eddy viscosity. Guohou and Peisheng [4] simulated local scouring downstream of a stilling basin by solving simultaneously, equations of motion and continuity equations for bed-load transport (Einstein equation) and for the bed material. Ushijima *et al.* [5] considered two- and three-dimensional scouring by warmed jets solving the unsteady continuity and momentum equations by using the k–ε turbulence closure model and the finite difference method. Ushijima [6] used an arbitrary Lagrangian–Eulerian approach in which three-dimensional body-fitted coordinates were generated for the sand bed profile, as it was unsteadily deformed by the flow.

Hoffmans and Booij [7] modelled the flow in a trench based on the solution of the two-dimensional Reynolds and the convection–diffusion equation, and computed the bed-load and suspended-load by using the stochastic method proposed by Van Rijn [8]. Olsen and Melaaen [9] predicted local scour developing processes using a three-dimensional flow and sediment transport model by solving the Reynolds equations with the k–ε model for turbulence closure. Hogg *et al.* [10] developed an analytical model predicting local scour of an initially flat bed of grains by two-dimensional turbulent wall jet by integrating a sediment-volume conservation equation.

Olsen and Kjellesvig [11] modelled the water flow around a circular cylinder placed vertically in a flume by using k–ε turbulence model in solving the Navier–Stokes equations, they solved the water flow field simultaneously with the sediment calculation. Hoffmans [12] applied Newton's second law of motion to derive relations for the maximum depth of scour by plunging or horizontal jets when no bed protection was present in the equilibrium phase. Garcia-Martinez *et al.* [13] presented a two-dimensional computational model to simulate suspended sediment transport and bed changes using the standard k–ε turbulence model. Karim and Ali [14] simulated the flow patterns generated by turbulent water jets impinging on rigid horizontal and scoured beds by three-turbulence closure models incorporated in FLUENT CFD package.

Salehi-Neyshabouri *et al.* [2] simulated the scouring process caused by a wall jet without a solid apron. Jia *et al.* [15] developed a numerical model, simulating the local scour in a plunge pool of loose bed due to a two-dimensional plane impinging jet by solving the flow field by CCHE3D, a finite element-based unsteady three-dimensional model, with a k–ε turbulence model. Salehi-Neyshabouri *et al.* [16] simulated scour by a free falling two-dimensional jet on cohesionless alluvium by solving the momentum, continuity and the k–ε equations for turbulent flows. Soulis [17] developed a fully coupled two-dimensional, viscous, free surface flow numerical model to calculate bed variations in alluvial channels. Gunal and Guven [1] simulated the turbulent flow patterns of water issued on frozen scoured beds using the standard k–ε model. Adduce and Sciortino [18] developed an analytical–numerical model that simulated local scour downstream of a sill followed by a rigid apron.

The above-mentioned studies can be classified according to their method of computing of shape of mobile bed. A group of them first solved the flow due to turbulent jet issuing on erodible soil together with the sediment distribution. Knowing the flow field and sediment concentration, they computed the shape of mobile bed due to the imbalance of sediment transport rate [2, 4–7, 11, 13, 16]. The second group directly computed the shape of instantaneous scour profile using a mass continuity equation for solid discharge [10, 12, 18, 19]. The latter group considered the external forces acting on sediment and related the net force causing the transport of sediment to

DOI: 10.1002/fld

imbalance between the hydrodynamic shear stress and the resistance of bed material. This approach is more realistic regarding the nature of the scour process. On the other hand, the former group computed the scour profile based on a mass balance between the sediment entering the scoured zone and that leaving the scoured zone. The transport of sediment concentration was computed by stochastic methods, based on past experimental data. This study differs from all previous ones in that it presents an alternative quasi-steady hybrid model, which co-operates two separate numerical methods in simulation of temporal evolution of scour profile and the flow patterns in and around the scoured zone.

This study presents a hybrid numerical–mathematical model, which simulates the temporal evolution of scour profile and flow patterns in scoured zone downstream of a sill followed by a rigid apron. The model contains a mathematical module computing instantaneous scour profile beneath horizontal jets, and a numerical module, which simulates the two-dimensional laterally averaged flow patterns in scoured zone for any time increment, assigned by the mathematical module. The developed hybrid model is validated by experimental data of past experimental researches.

2. THE PROPOSED HYBRID MODEL

The hybrid numerical–mathematical model contains two modules, namely a mathematical module computing the shape of scour hole for a pre-defined time increment, Δt, and a numerical module simulating the two-dimensional laterally averaged flow patterns in computed scoured zone. Two modules are interconnected to each other by a quasi-steady time-stepping mechanism: first the mathematical module solves a time-dependent integro-parabolic equation, whose unknown is the ordinate of scour hole $S_l(x,t)$. Then, the numerical module gets the computed scour profile, and calculates the internal flow characteristics in the scoured zone for the corresponding time interval $(n \times \Delta t)$. These two modules are connected to each other at the computational program level.

2.1. The numerical module

The numerical module is based on the solution of two-dimensional continuity and momentum equations, shown below in tensor form

$$\frac{\partial u_i}{\partial x_i} = 0 \tag{1}$$

and

$$u_j \frac{\partial u_i}{\partial x_j} = -\frac{1}{\rho} \frac{\partial}{\partial x_j} (p\delta_{ij} + \overline{u_i u_j}) \tag{2}$$

where ρ is the mass density of water, δ_{ij} is the Kronecker delta ($\delta_{ij} = 1$ if $i = j$ and $\delta_{ij} = 0$ if $i \neq j$). The turbulent eddy viscosity (v_t) is modelled using the standard k–ε turbulence model

$$v_t = C_\mu \frac{k^2}{\varepsilon} \tag{3}$$

DOI: 10.1002/fld

where C_μ is an empirical constant. The standard k–ε model employs the Boussinesq eddy viscosity concepts for Reynolds stresses

$$-\overline{u_i u_j} = v_t \left(\frac{\partial u_i}{\partial x_j} + \frac{\partial u_j}{\partial x_i} \right) - \frac{2}{3} k \delta_{ij} \tag{4}$$

where u_i and u_j represent the mean velocity components, and x_i and x_j are the space coordinates. The distributions of k and ε are determined from

$$u_j \frac{\partial k}{\partial x_j} = \frac{\partial}{\partial x_j} \left(\frac{v_t}{\sigma_k} \frac{\partial k}{\partial x_j} \right) + \frac{\partial}{\partial y} \left(\frac{v_t}{\sigma_k} \frac{\partial k}{\partial y} \right) + G - \varepsilon \tag{5}$$

$$u_j \frac{\partial \varepsilon}{\partial x_j} = \frac{\partial}{\partial x_j} \left(\frac{v_t}{\sigma_k} \frac{\partial \varepsilon}{\partial x_j} \right) + \frac{\partial}{\partial y} \left(\frac{v_t}{\sigma_k} \frac{\partial k}{\partial y} \right) + G - C_1 \frac{\varepsilon}{k} G - C_2 \frac{\varepsilon^2}{k} \tag{6}$$

where σ_t is the turbulent Prandtl/Schmidt number ($\sigma_t = 0.7$) and G is the turbulence energy production term and defined as,

$$G = v_t \frac{\partial u_i}{\partial x_j} \left(\frac{\partial u_j}{\partial x_i} + \frac{\partial u_i}{\partial x_j} \right) \tag{7}$$

The turbulence model coefficients, $\sigma_k = 1.0$, $\sigma_\varepsilon = 1.3$, $C_1 = 1.44$, $C_2 = 1.92$ and $C_\mu = 0.09$, were determined from the results of some specific experiments and computational optimization [20, 21].

2.2. Boundary conditions

At the inlet, the streamwise velocity u is assumed to be uniform and vertical velocity v is assumed as zero for the cases of sluice gate without apron, whereas for the cases of hydraulic structures followed by a rigid apron, the streamwise velocity u is calculated using the exponential equation proposed by Karim and Ali [14], which was developed based on the experimental and theoretical study of Rajaratnam and Berry [22].

$$\frac{u}{u_m} = \mathrm{e}^{-0.693(y/\delta)^2} \tag{8}$$

where u_m is the maximum velocity of the velocity profile at any x distance from the inlet, and y is the vertical distance from the axis of jet at any x direction, $\delta = 0.7x$ is the vertical distance from the axis to the point where $u = u_m/2$.

Zero pressure gradient is assumed in the streamwise direction next to the inlet. With the assumption of turbulence being locally isotropic and in equilibrium at the inlet, turbulence quantities k and ε are taken from the experimental measurements of Long *et al.* [23] as,

$$k_{\text{inlet}} = 1.4 \times 10^{-3} u_1^2 \tag{9}$$

$$\varepsilon_{\text{inlet}} = 2.2 \times 10^{-5} \frac{u_1^3}{y_1} \tag{10}$$

At the outflow boundary, zero-gradient boundary conditions are used and velocities are set equal to the values in the elements closest to the outflow.

$$\frac{\partial U}{\partial x} = \frac{\partial V}{\partial x} = \frac{\partial k}{\partial x} = \frac{\partial \varepsilon}{\partial x} = 0 \tag{11}$$

DOI: 10.1002/fld

The velocity normal to the free surface and the pressure on the surface are taken to be zero. First derivatives of U, V, k and ε with respect to η are taken to vanish on the free surface. Thus, the surface conditions are:

$$P_{\text{surface}} = 0 \tag{12}$$

$$V_{\text{surface}} = 0 \tag{13}$$

$$\frac{\partial U}{\partial y} = \frac{\partial V}{\partial y} = \frac{\partial \varepsilon}{\partial y} = \frac{\partial k}{\partial y} = 0 \tag{14}$$

The free surface is adjusted at the end of each iteration, using the closest three nodes to free surface in computational domain. Then the free surface for the next iteration is adjusted according to the piezometric pressure distribution ($P_{\text{atmospheric}} + \rho g z$).

Wall functions, proposed by Launder and Spalding [24], are applied in the near wall region, which rely on the existence of the logarithmic region in the velocity profile. Implementation of wall boundary conditions for turbulence model is accessed by evaluating the scaled wall distance, y^+, between the wall surface and the computational node nearest the wall. For distances where $y^+ \geqslant 11.63$, the flow is turbulent and the wall function approach is used, for y^+ values less than 11.63 the near wall flow is taken as laminar. From this assumption and the eddy viscosity formula, the following wall functions are developed:

$$u^+ = \ln(E y^+)/\kappa, \quad k_{\text{wall}} = u_*^2/(C_\mu)^{0.5} \tag{15}$$

where $\kappa = 0.41$ is the Von Karman constant, E is a wall roughness parameter $= 9.0$ (in present study, E value is shifted between 8.5 and 9.0 for calibration purpose), $u^+ = u/u_*$; $y^+ = y u_*/v$ and u_* is the friction velocity defined by $u_* = (\tau_w/\rho)^{1/2}$ where τ_w is the wall shear stress. An iterative technique proposed by Benim and Zinser [25] is used for the wall shear stress model.

2.3. *Boundary-fitted coordinates*

The governing equations presented in this study are in cartesian coordinates. However, owing to the curvature of the free and bed surfaces, a cartesian coordinate system is less effective as approximations have to be made at the surface for a rectangular grid. Such approximations make it necessary to use fine mesh in cartesian coordinates, but this is computationally expensive. In order to overcome this difficulty, the continuity and momentum equations with transport equations were transformed into the boundary-fitted coordinate system as

$$\xi = x \tag{16}$$

$$\eta = \frac{y - y_o}{y_t - y_o} \tag{17}$$

where ξ and η are the coordinates of the transformed plane and y_o is the ordinate of the bed profile for the correspondent ordinate value, y, of any point in physical plane and y_t is the tailwater depth. In this way, we will transform the independent variables in the physical plane (x, y) to a new set of independent variables in transformed plane (ξ , η). By this, we avoid the irregularities on the free surface and the wall boundaries. Then, we re-transform the solved governing equations to physical plane by using transformation equations (see [1]).

DOI: 10.1002/fld

For instance, the continuity equation (Equation (1)) can be rewritten in the (ξ, η) coordinates as

$$\frac{\partial U}{\partial \xi} + \frac{\partial V}{\partial \eta} = 0 \tag{18}$$

where U and V are velocity components in the computational plane.

After the free surface is adjusted, the grid mesh in the physical plane is corrected using the new free surface elevation, and the corresponding computational domain is re-generated using Equations (16) and (17).

2.4. Numerical solution of the partial differential equations

The finite volume method was chosen for discretization and integration of transformed governing equations, because it is easy to implement and conservation can always be obtained in the computational cells. A grid system is first generated numerically at the corner of each control volume. The velocities are calculated at a point halfway between these grid nodes and the pressures are calculated at the centre of each control volume. This staggered grid system is adopted for variable arrangement to avoid the well-known chequerboard oscillations in pressure and velocity. Since a staggered grid system is employed for all velocity components (U, V) and scalar quantities (p, k, ε), a separate control volume is to be considered for the integration of each governing equations. The integration of the transformed governing equations for a dependent variable is described in a general form as [21]

$$A_p \Phi_p = A_E \Phi_E + A_W \Phi_W + A_N \Phi_N + A_S \Phi_S + S_\Phi \tag{19}$$

where Φ represents any dependent variable (u, v, p, k or ε), the subscripts P, E, W, S and N stand represent direction of grid point (see Figure 1), and S is the source term.

The hybrid differencing scheme proposed by Patankar and Spalding [26] has been used in discretization of governing equations. The system of equations is solved by tri-diagonal matrix algorithm, a line iterative method, with alternating sweep directions. In an iterative scheme, it is often desirable to speed up or slow down the changes of dependent variables from iteration to iteration, which is known as over-relaxation or under-relaxation. Because the Navier–Stokes

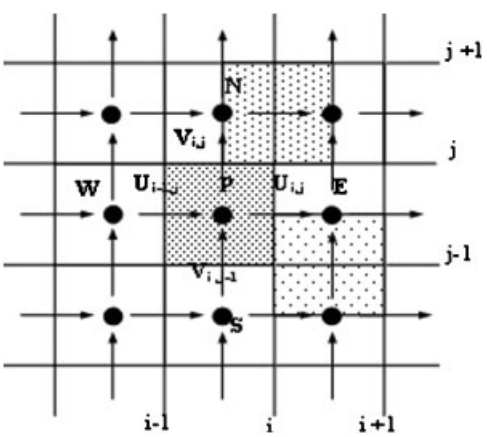

Figure 1. Control volumes in computational domain.

DOI: 10.1002/fld

Table I. Under-relaxation factors for experimental conditions.

	Under-relaxation factor (Ω_i)						
Test	Ω_u	Ω_v	Ω_p	Ω_s	Ω_h	Ω_d	Ω_k
A1–A2	0.5	0.5	0.3	0.3	0.3	0.2	0.2
A3–A4	0.3	0.3	0.2	0.2	0.2	0.1	0.1

equations are non-linear, the process of convergence needs to be slowed down. In the present study, in order to avoid divergence, under-relaxation factor ($0<\Omega<1$) with changeable values in each run of program was used for velocities and pressures. The values of Ω for each dependent variable are given in Table I, for each test used for simulation. It should be noted that the under-relaxation factors are mainly problem dependent and have no influence on the converged solution.

The pressure gradients, present in the momentum equations calculated using SIMPLE algorithm, which stands for semi-implicit method for pressure-linked equations, as described by Patankar and Spalding [26] and Patankar [21].

2.5. The mathematical module

The temporal scour profile is computed from a two-dimensional continuity equation for local solid discharge together with the mechanical properties of the sand subjected to scouring (Equation (3.72)), whose unknown is $S_l(x,t)$. The model analyses the forces acting on a sand particle, considering the angle of repose of the sand (φ), the critical shear stress beyond which the particle is dislodged (τ_{cr}), and the hydrodynamic shear stress induced by the impinging water jet (τ_{hydr}). Adduce [19] proposed the continuity equation for solid discharge as

$$\frac{\partial S_l}{\partial t}+\left(\frac{1}{1-p}\right)\frac{\partial}{\partial x}\left(\frac{Q_{\mathrm{sd}}}{\sqrt{1+S_{lx}^2}}\right)=0 \tag{20}$$

where S_{lx} is the derivative of S_l with respect to the x-axis, p is porosity of sand and Q_{sd} is the solid discharge. Equation (20) represents a conservative form and includes unresolved differential terms. As Adduce [19] also admits, differentiating all terms in Equation (20) using chain rule would give a more accurate model. Referring to Equations (20) and (21), it is obvious that differentiating Equation (20) revealed gradient and time derivatives of most affective parameters Q_{sd}, τ_{hydr}, which do not exist in Equation (20). The derivative terms included in Equation (20) were solved using chain rule and the following non-conservative differential equation was obtained:

$$\frac{\partial S_l}{\partial t}+\frac{1}{1-p}\left[\frac{\partial Q_{\mathrm{sd}}/\partial\psi}{\sqrt{1+S_{lx}^2}}\left(\frac{\partial\tau_{\mathrm{hydr}}}{\partial x}-\frac{\tau_{\mathrm{cr}}(1-\tan(\varphi)\,S_{lx})}{\tan(\varphi)\,(1+S_{lx}^2)^{3/2}}\frac{\partial^2 S_l}{\partial x^2}\right)-Q_{\mathrm{sd}}\frac{\partial S_l}{\partial x}\frac{\partial^2 S_l/\partial x^2}{(1+S_{lx}^2)^{3/2}}\right]=0 \tag{21}$$

We used the Meyer–Peter and Muellller transport formula [27]

$$\begin{aligned} Q_{\mathrm{sd}} &= \frac{8}{\sqrt{\rho}(\gamma_s-\gamma)}\psi^{3/2} \quad \text{for } \psi>0 \\ Q_{\mathrm{sd}} &= 0 \quad \text{for } \psi\leqslant 0 \end{aligned} \tag{22}$$

DOI: 10.1002/fld

where,

$$Q_{sd} = f(\psi) \quad \text{where } \psi = \tau_{hydr} - \frac{\tau_{cr}(\tan(\varphi) + S_{lx})}{\tan(\varphi)\sqrt{1 + S_{lx}^2}} \tag{23}$$

and ψ is an independent variable.

The hydraulic bed shear stress is calculated, taking into account the Gaussian law proposed by Hogg *et al.* [10] as

$$\tau_{hydr} = \frac{\rho \alpha C_1^2 q^2}{N_i^{1/4}(2.49\ln(13.3Rf_r/d_{50}))^{1/4}(x/L_p)(y_t - S_l)} G(x, S_l) \tag{24}$$

where $\alpha = 0.00283$ is a numerical constant, $N_i = 11.5$ is the Nikuradse number, R is the hydraulic radius and f_r is the shape factor of channel cross-section (f_r = width of channel/height of channel), C_1 is a constant, which is calculated by the measured velocity profile of the wall jet at the end of apron, y_t is tailwater depth and L_p is length of rigid apron. $G(x, S_l)$ is the Gaussian term, used for simulating the different transport action of the free jet from the edge of apron until maximum scour depth abscissa (XS) and that of a wall jet from that point till the end of dune section. Namely, the Gaussian function becomes weaker when simulating the free-like jet and becomes stronger and stronger as the free jet changes into wall jet as

$$G(x, S_l) = \begin{cases} 1 & \text{for } x > XS \text{ or in absence of scour} \\ \exp\left(-\left[\dfrac{x - XS}{XS}\right]^2 \ln(1/\varsigma)\right) & \text{for } x \leqslant XS \text{ or in presence of scour} \end{cases} \tag{25}$$

where $G(0, S_l) = \varsigma$, $0 < \varsigma < 1$ is a calibration parameter of the proposed model, which considers the transport action of free jet is weaker than that of wall jet in the region of the end of rigid apron.

The proposed mathematical model, Equation (21) has a parabolic partial differential structure. Thus, the integration of the equation requires specific numerical integral methods with implication of proper boundary conditions. Following Garcia and Kahawita [28] and Adduce [19], we used a MacCormack Scheme in numerical integration of Equation (21) with two difference operators, namely backward (B) and forward (F) functioning as

$$B(S_l)_i^n \equiv \frac{(S_l)_i^n - (S_l)_{i-1}^n}{\Delta x} \tag{26}$$

$$F(S_l)_i^n \equiv \frac{(S_l)_{i+1}^n - (S_l)_i^n}{\Delta x} \tag{27}$$

where $(S_l)_i^n \equiv S_l | x = i\Delta x, t = n\Delta t$, i and n are spatial and temporal indexes, respectively, used in the present scheme. $\Delta x = L/M$ is the spatial step of integral, M is the number of the discretization and Δt temporal step of integration. In this study, M is taken as 100 and Δt as 0.02 s.

The empirical relationship for hydraulic shear stress (Equation (24)) is also used as the initial value for calculating the wall shear stress in numerical module. Then the numerical module updates the wall shear stress (τ_w) by iteration as proposed by Benim and Zinser [25].

DOI: 10.1002/fld

The proposed MacCormack scheme uses a predictor–corrector numerical scheme according to following integration scheme:

$$(S_l)_i^P = (S_l)_i^n - \Delta t\left(\frac{1}{1-p}\right)B\left[\frac{\frac{\partial Qs}{\partial x}\sqrt{1+F(S_l)_i^n} - Qs\left(\frac{1}{2}(1+F(S_l)_i^n)^{-1/2}\left(\frac{\partial F(S_l)_i^n}{\partial x}\right)\right)}{1+F(S_l)_i^n}\right] \tag{28}$$

$$(S_l)_i^C = (S_l)_i^p - \Delta t\left(\frac{1}{1-p}\right)F\left[\frac{\frac{\partial Qs}{\partial x}\sqrt{1+B(S_l)_i^p} - Qs\left(\frac{1}{2}(1+B(S_l)_i^p)^{-1/2}\left(\frac{\partial B(S_l)_i^p}{\partial x}\right)\right)}{1+B(S_l)_i^p}\right] \tag{29}$$

$$(S_l)_i^{n+1} = \frac{1}{2}((S_l)_i^C + (S_l)_i^n) \tag{30}$$

where P and C stand for the predictor and the corrector step, respectively.

As explained before, the numerical integral algorithm explained above needs be to closed by using appropriate boundary conditions. These boundary conditions are namely clear-water scour condition at the inlet of the mobile bed and absence of the local solid discharge at the end of it ($x=0$ and $x=L$).

The clear-water condition at the inlet and at the end of the mobile bed is defined as

$$\tau_{\text{hydr}}(S_l) = \lambda\tau_{\text{eff}}(S_{lx}) \tag{31}$$

where $\tau_{\text{eff}} = \tau_{\text{cri}} - \tau_s$ is the effective shear resistance of sediment and λ is a model parameter, the value of which should be properly chosen. In this study, the values of λ are calibrated according to experimental results. The clear-water condition at the inlet is discretized as

$$\tau_{\text{hydr}}(S_l)_0^{n+1} = \lambda_0\tau_{\text{eff}}(B(S_l)_1^{n+1}) \tag{32}$$

where $(S_l)_1^{n+1}$ is known, since it is calculated in the internal grid point. Thus, in the above equation the only unknown is $(S_l)_0^{n+1}$. Equation (32) can be numerically solved for assigned the value of λ_0.

At the outlet boundary, zero-gradient boundary condition is used and the hydraulic shear stress is set equal to the value in the element closest to the outlet

$$\tau_{\text{hydr}}(S_l)_m^{n+1} = \tau_{\text{hydr}}(S_l)_{m-1}^{n+1} \tag{33}$$

where the only unknown is $(S_l)_m^{n+1}$ and is equalized to $\tau_{\text{hydr}}(S_l)_{m-1}^{n+1}$ value.

3. VALIDATION OF THE MODEL

In order to validate the hybrid model and evaluate its general performance, the model is run for various experimental tests (10 tests) carried out by Adduce [19], but only the simulations for four tests (see Table II) are illustrated in this study. The first application concerns the simulation of temporal scour profile and also the prediction of asymptotic scour profiles. The second one

DOI: 10.1002/fld

Table II. Experimental conditions used in model validation.

Test	Q (m^3/s)	U_1 (m/s)	h_s (m)	y_t (m)	S_{max} (m)	L_s (m)	T (min)
A1	0.0123	3.074	0.023	0.129	0.044	0.375	580
A2	0.0162	3.089	0.026	0.137	0.061	0.600	480
A3	0.0184	3.072	0.028	0.143	0.067	0.630	580
A4	0.0263	3.146	0.033	0.156	0.082	0.800	450

concerns the simulation of flow patterns, namely mean velocity distribution, free surface profiles, and Reynolds stress distributions over the rigid apron followed by a sill, and the scour profile including the dune section. The predictions of the proposed hybrid model to the measured ones are illustrated in the figures.

3.1. Adduce [19]'s experiments: Local scour downstream of a sill followed by rigid apron

The experiments of Adduce [19] were carried out in a 17 m long flume with a rectangular cross-section of 1 m height and 0.8 m width, with a 0.3 m high, 0.8 m wide and 3 m long test section. A mobile bed of uniformly graded sand of mean diameter $d_{50}=0.72\,mm$, $d_{90}=0.96\,mm$, density $\rho_s=2650\,kg/m^3$ and a porosity $p=0.44$ was used in the tests. In order to produce a bed of homogeneous roughness, the same sand was glued both to the upstream and downstream fixed-bed sections. Clear-water scour conditions were conducted by supplying no sediment into scour zone. A sill of height $z=0.15\,m$, followed by a rigid apron of length $Lp=0.5\,m$ was installed upstream of the test section. The downstream water depth was controlled using a control gate at the end of the flume. The water levels in the flume were measured with a point gauge of accuracy $=0.10\,mm$ was mounted on a carriage, which moved along the flume. The water discharge at the inlet was measured with an electromagnetic flow-metre and controlled by an inlet valve. The movement of the sand bed was prevented by increasing the water discharge slowly and setting to the desired experimental value.

The water discharge (Q) was kept constant for the entire duration of the experiment. The evolution of the scour hole was recorded by a charge-coupled device camera connected to a digital videocassette recorder. A detailed study of the temporal evolution of the scour hole was made possible by an image analysis technique (see [19]). The experiments were stopped when the measured maximum scour depth, plotted vs log time was sensibly constant. At the end of the experiment velocity measurements were performed by an ultrasonic doppler velocimeter. The experimental conditions, which are used in this study, are given in Table II. In Table II, also the maximum scour depth values (S_{max}), the maximum scour length (L_s), inlet velocity entering the mobile bed section, U_1, and the test duration (T) for each test are reported.

4. THE PHYSICAL AND COMPUTATIONAL DOMAINS

As an example, the actual grid mesh in the physical domain and the computational domain are given in Figure 2, for test A1 by Adduce [19]. The absolute size of the cells within the grid is an important issue, since if the cells are too large the solution obtained can be dependent on the cell size rather than on the physical conditions of the solution domain and input conditions [29]. For all experimental conditions, a grid arrangement of 101×51 was used. It can be easily observed from

DOI: 10.1002/fld

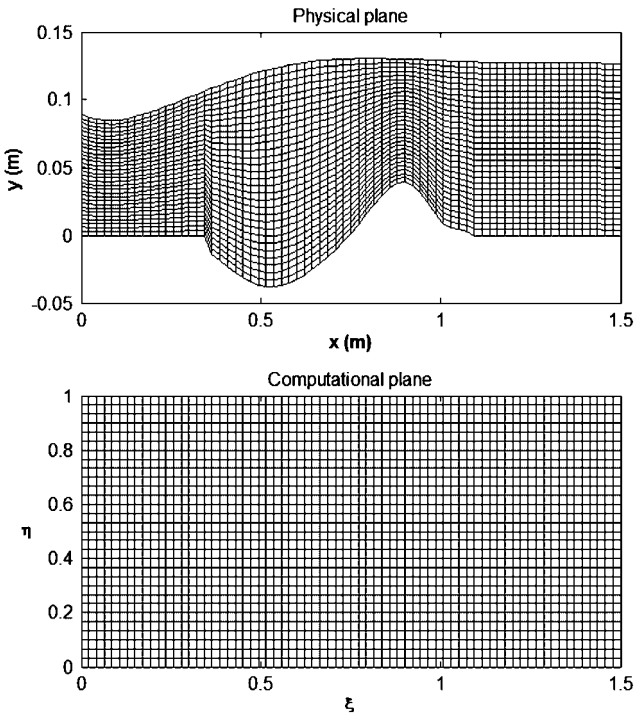

Figure 2. Grid transformation for test A1.

the figure that, although the shape of the physical domain varies for different physical conditions, the computational domain is always rectangular. In other words, the physical domain is likely stretched in vertical axis and the horizontal axis is fixed. Hence, it makes easy to discretize the governing equations (Equations (1)–(7)). Moreover, the boundary conditions (Equations (8)–(15)) are able to be applied much more easily without any interpolation on the boundary cells as needed when the physical domain is used as the solution domain.

5. THE CONVERGENCE

The model is run for a pre-defined duration according to the simulated experimental test condition. After the mathematical module is converged, the shape of temporal scour profile is transferred to the numerical module. The convergence of the numerical module is monitored by the absolute residual sum for the continuity equation (Equation (18)) for the solution domain. The program stops when the residual sum is 0.0001 or the iteration number, ii, reaches a value pre-defined by the user. For iteration purpose, a computer program is written in Fortran 90, by Developer Studio, a visual fortran developing software. The iterations are carried out using the super-computer, which utilizes the Linux Kernel 2.6 operation system with Intel Core 2 6600 at 2.4 GHz processor and 3.3 giga-bytes memory.

DOI: 10.1002/fld

6. RESULTS AND DISCUSSION

6.1. Temporal scour profiles

The time evolution of scour profiles for the three experimental runs carried out by Adduce [19], the tests A1, A2 and A4, is simulated by the proposed hybrid model. For the tests A1 and A2, the predictions for eight time increments, $t = 10, 50, 100, 200, 300, 400, 500$ and 600 are presented (see Figures 3 and 4) and for the test A4, the evolution of scour profile for seven time increments, $t = 10, 50, 100, 200, 300, 400, 500$ min are presented (see Figure 5). As a general view from Figures 4–6, the geometry of the scour hole increases with increasing flow rates. As Adduce [19] also admits, for small flow rates, a small dune with sharp crest follows the scour hole and by increasing the flow rate, the dune becomes flatter and longer. Adduce [19] observed that the effect of the smooth side-wall on scouring and on the flow field was negligible, as the channel width was 0.8 m, being sufficient to reduce the side-wall effect and pointed out the symmetry of scour profiles with respect to the centreline of the flume, which was measured at five different longitudinal sections.

Figures 6–8 show the proposed model's predictions to the measured asymptotic scour profiles of tests A1, A2 and A4, respectively. From the figures, perfect agreement is observed between the predicted and the experimental scour profiles, especially in scoured zone. But the numerical

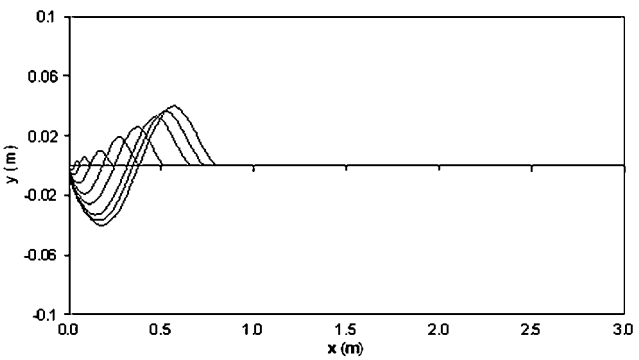

Figure 3. Predicted temporal evolution of local scour for test A1.

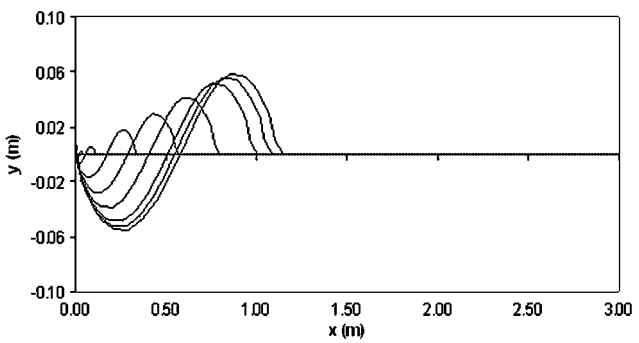

Figure 4. Predicted temporal evolution of local scour for test A2.

DOI: 10.1002/fld

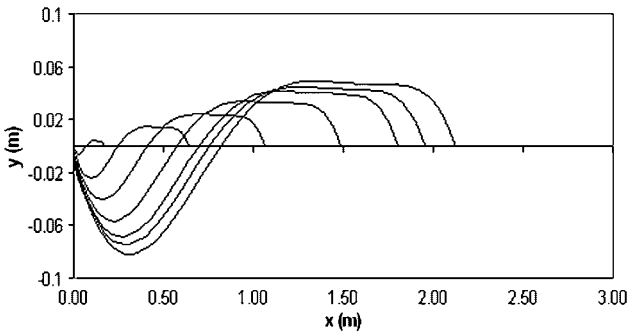

Figure 5. Predicted temporal evolution of local scour for test A4.

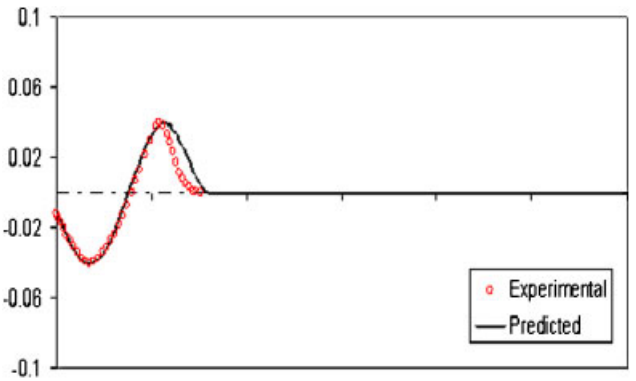

Figure 6. Predicted scour profile vs measured one for test A1.

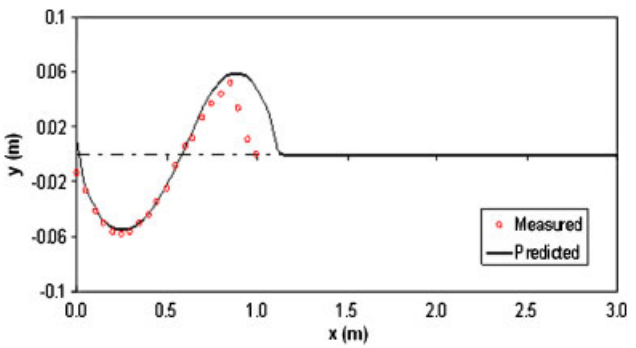

Figure 7. Predicted scour profile vs measured one for test A2.

predictions of the dune section are observed to be longer than the measured ones for small flow rates (tests A1–A2) (see Figures 6 and 7), and for high discharges (A4), only very small discrepancies are observed between the predicted and the measured ones (see Figure 8). It can be concluded that

DOI: 10.1002/fld

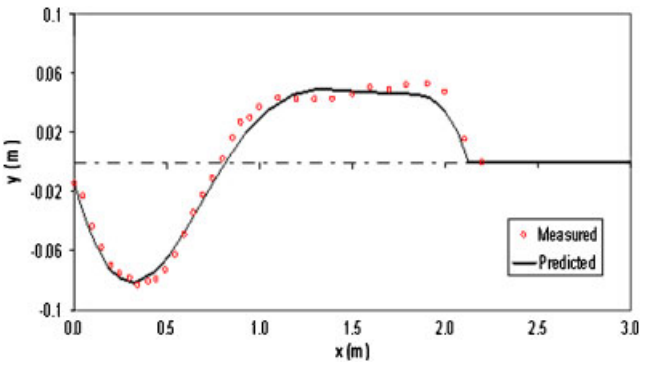

Figure 8. Predicted scour profile vs measured one for test A4.

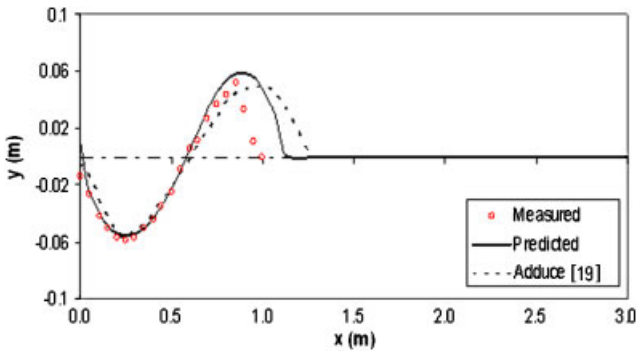

Figure 9. Comparison of predicted and scour profiles for test A2.

when the flow rate increases, the numerical predictions of the dune section get better, compared with the measured ones and the numerical predictions of the dune section for small discharges are always longer than the measured ones. This event was also observed by Adduce [19] and it can be attributed to the fact that the predicted scour profiles are two-dimensional, although the experimentally observed ones are quasi-two-dimensional when the flow rates are large (test A4), but no more quasi-two-dimensional for small flow rates (tests A1–A2) [18, 19].

Figures 9 and 10 show the predicted scour profiles of the present model and the analytical model proposed by Adduce [19] compared with the measured asymptotic scour profiles of the tests A2 and A4. As explained in the previous sections, our proposed numerical model calculates the non-conservative form of the equation for temporary scour profile (Equation (21)) while the model by Adduce [19] calculates Equation (20), which is the conservative form of the Equation (21). By this, we expect to achieve more realistic and accurate predictions. From both figures, it is obvious that the predictions of our model are closer to the measured ones, compared with those of the model by Adduce [19] especially in predicting the dune section for small discharge (test A2). It has been observed that the proposed model predicted the measured scour profile with higher accuracy ($R^2 = 0.964$) and lower error (MSE $= 0.0001$) when compared with the analytical model by Adduce [19] ($R^2 = 0.924$, MSE $= 0.0020$).

DOI: 10.1002/fld

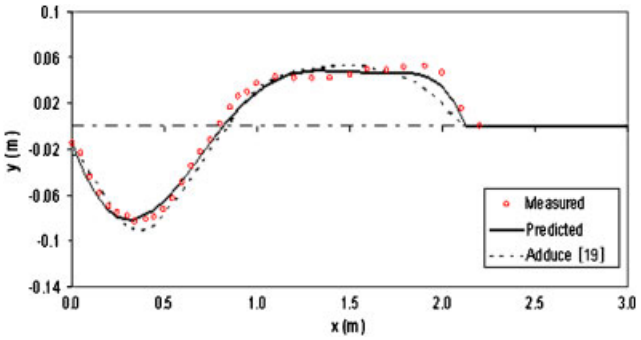

Figure 10. Comparison of predicted and scour profiles for test A4.

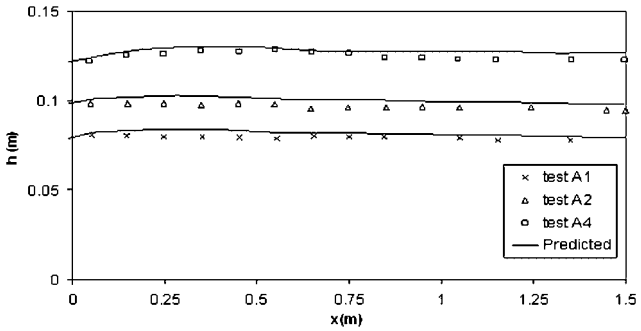

Figure 11. Predicted free surface profiles vs measured ones.

6.2. *Free surface profiles*

Figure 11 shows the predictions of free surface profile to the experimental ones measured by Adduce [19] for tests A1, A2 and A7, at asymptotic stages. At the inlet of the scour profile, the surface profiles start to jump until a peak in the region of $0<x<0.5$. Downstream of this region ($x>0.5$ m), the flow decreases steadily and then the rate of variation is observed to approach zero. It is obvious that the proposed hybrid model predicted the measured free surface profiles with quite good agreement.

6.3. *Dimensionless velocity profiles*

Figures 12 and 13 show the predicted and measured dimensionless velocity profiles and the theoretical curve of a wall jet proposed by Rajaratnam [30] along the region $XS<x<L$, for tests A2 and A4, respectively. The velocities are normalized by u_m and the y-axis by δ. Almost perfect agreement is observed between the predicted and the measured dimensionless velocity profiles for $0.2<y/\delta<1.0$ and a fairly good one for $1<y/\delta<2$. The predicted and the measured dimensionless velocity profiles for $0.2<y/\delta<1.0$ are observed to be over the theoretical curve, whereas they are totally below the theoretical curve for $1<y/\delta<2$. The small discrepancies for $1<y/\delta<2$ can be explained by under-predictions of the standard k–ε turbulence model, especially in reverse flow

DOI: 10.1002/fld

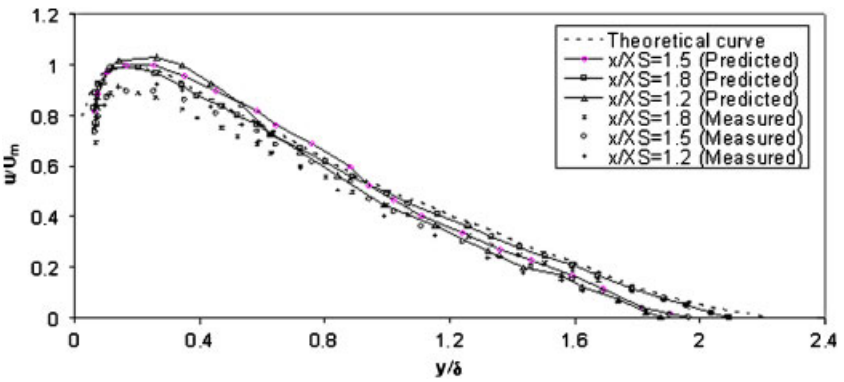

Figure 12. Predicted and measured dimensionless velocity profiles vs theoretical curve for A2.

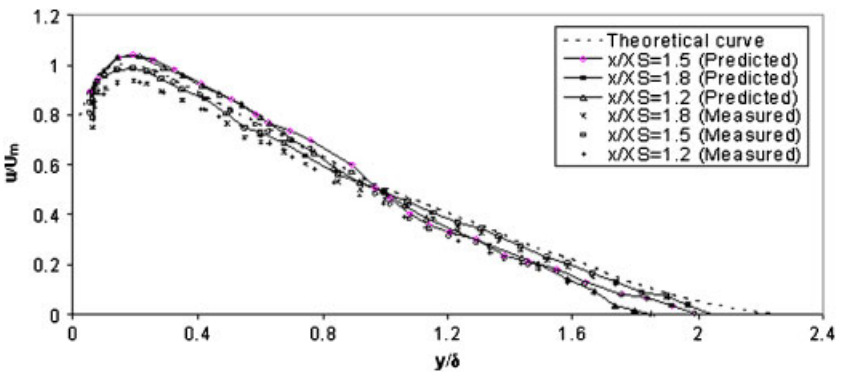

Figure 13. Predicted and measured dimensionless velocity profiles vs theoretical curve for A4.

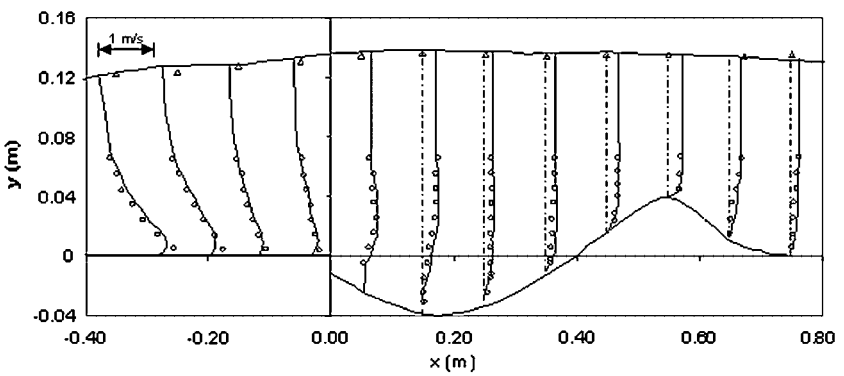

Figure 14. Predicted and measured u-velocity distribution over the rigid apron and scour profile for test A1.

DOI: 10.1002/fld

regions. Both predicted and measured dimensionless velocity profiles can generally be said to be similar to the theoretical wall jet.

6.4. *Velocity distribution in scoured zone*

In this section the experimental velocity profiles (u, v) for runs A1 and A3, measured by Adduce [19], are compared with the numerical predictions of the proposed model. Figures 14–17 show the present model's predictions of velocity distribution and the measured ones by Adduce [19]. The dots ($\circ$) represent the measured velocity, triangles (Δ) represent the measured surface profiles and the solid lines (-) represent the predictions of the present model to the measured ones. From Figures 14–17, it is obvious that the horizontal component (u) of flow velocity is higher than the vertical one (v) throughout the whole scour profile. In Figures 14 and 16, for the tests A1 and A3, it can be observed that the maximum velocity increases from the maximum scour depth region to the crest of dune, while it decreases beyond the crest of the dune. As a general view, it can be concluded that the flow from the maximum scour depth to the end of the dune can be modelled by plane wall jet analogy [19, 30–32].

As it is seen in Figures 14 and 16, for $0 \leqslant x \leqslant XS$, where $XS = 0.174$ for run A1 and $XS = 0,285$ for run A3, the jet behaves like a free jet, the erosive action of which is very weak compared with the wall jet. Beyond this zone to the end of the dune section, the flow becomes a wall jet that erodes more aggressively and deepens the scour area faster. Figures 14–17 prove that the numerical predictions of the proposed model are in good agreement with the above findings by the experimental data measured by Adduce cite Adduce 2004. The weak effect of the free jet at the inlet of the scour hole is simulated based on a Gaussian-like relation as explained in previous sections.

6.5. *Distribution of Reynolds stresses*

The Reynolds stresses, $-\overline{u'^2}$ and $-\overline{v'^2}$ can be calculated from the measured $u\,(x, y, t)$ and $v\,(x, y, t)$ data using Boussinesq relation (Equation (4)). Figures 18–21 show the predictions of the present hybrid model to the spatial distribution of the Reynolds stresses, for the tests A1 and A3 measured

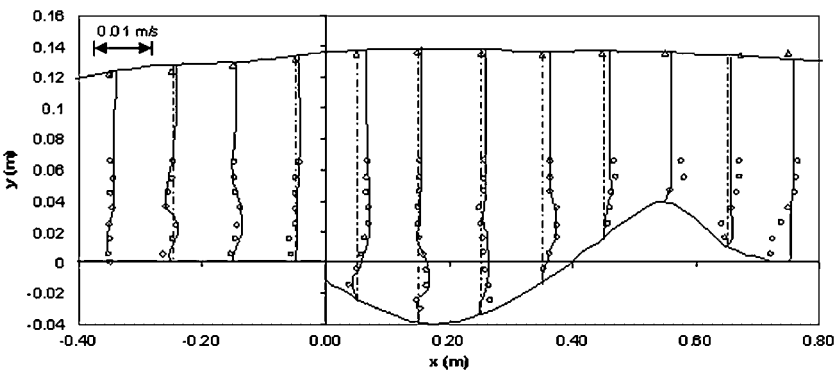

Figure 15. Predicted and measured v-velocity distribution over the rigid apron and scour profile for test A1.

DOI: 10.1002/fld

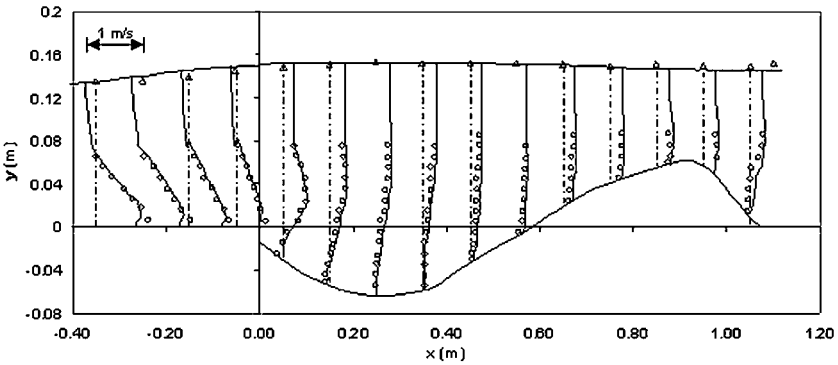

Figure 16. Predicted and measured u-velocity distribution over the rigid apron and scour profile for test A3.

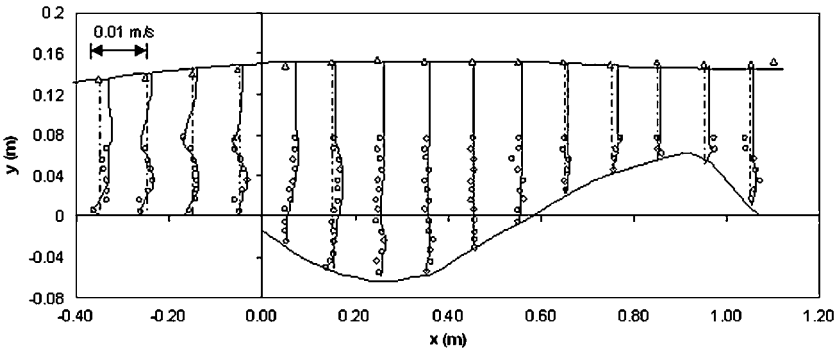

Figure 17. Predicted and measured v-velocity distribution over the rigid apron and scour profile for test A3.

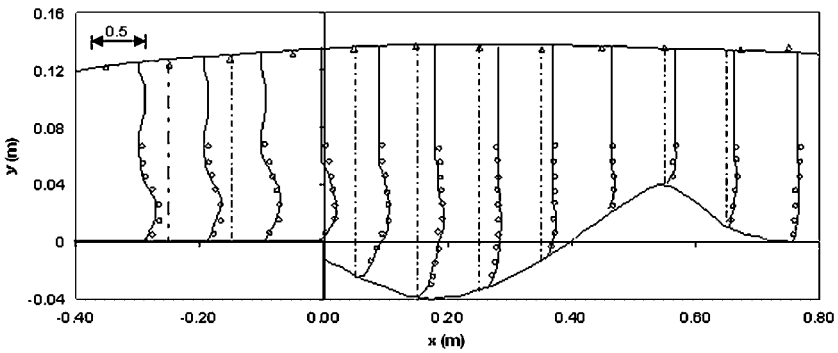

Figure 18. Predicted and measured $\sqrt{\overline{u'^2}}/U_0$ distribution over the rigid apron and scour profile for test A1.

DOI: 10.1002/fld

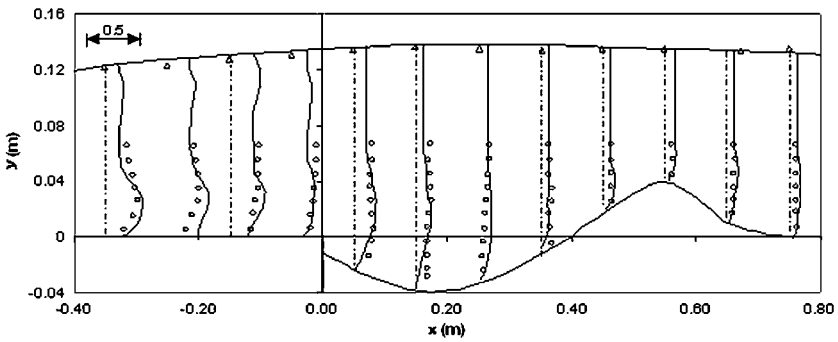

Figure 19. Predicted and measured $\sqrt{\overline{v'^2}}/U_0$ distribution over the rigid apron and scour profile for test A1.

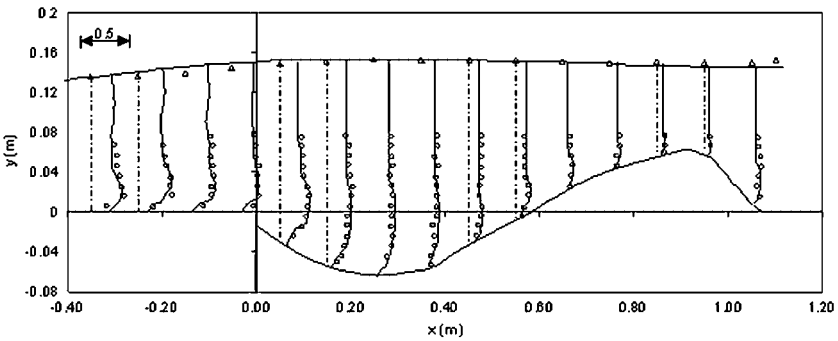

Figure 20. Predicted and measured $\sqrt{\overline{u'^2}}/U_0$ distribution over the rigid apron and scour profile for test A3.

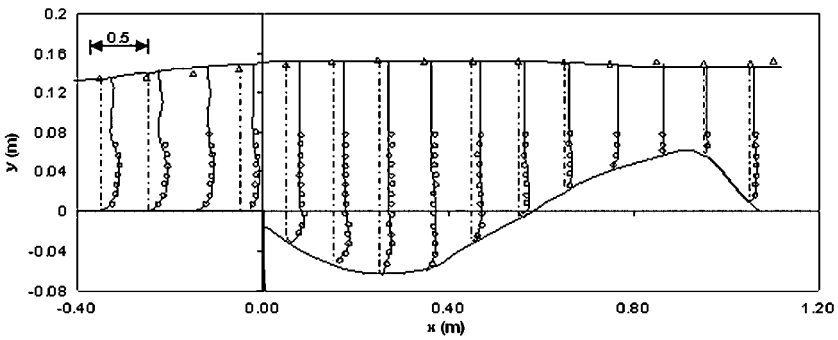

Figure 21. Predicted and measured $\sqrt{\overline{v'^2}}/U_0$ distribution over the rigid apron and scour profile for test A3.

DOI: 10.1002/fld

by Micro ADV at the flume centreline by Adduce [19]. The dots (∘) represent the measured velocity, triangles (Δ) represent the measured surface profiles and the solid lines (-) represent the predictions of the present model to the measured ones. The Reynolds stresses are made non-dimensional by velocity scale U_0 (defined in Equation (34)) and by the length scale y_0 in horizontal plane.

$$U_0 = \frac{Q}{b \times y_0} \tag{34}$$

As a general view, the numerical predictions compare well with the measured data. From the figures, both the numerical predictions and the measured data prove that the turbulent flow is non-isotropic since $\sqrt{\overline{u'^2}}$values are generally greater than $\sqrt{\overline{v'^2}}$ for the whole spatial distribution, ($\sqrt{\overline{u'^2}} = 1.6\sqrt{\overline{v'^2}}$), which is also observed by Adduce [19], Liriano *et al.* [33] and Gunal and Guven [1]. Liriano *et al.* [33] observed that $\sqrt{\overline{u'^2}} = 1.6\sqrt{\overline{v'^2}}$, where Gunal and Guven [1]'s predictions revealed that $\sqrt{\overline{u'^2}} = 1.69\sqrt{\overline{v'^2}}$, and Adduce [19]'s measurements gave out that $\sqrt{\overline{u'^2}} = 1.65\sqrt{\overline{v'^2}}$.

As a general view from Figures 18 and 20, as y increases, $\sqrt{\overline{u'^2}}$ increases till a maximum value, approximately at the point where the u-velocity distribution has also its maxima and then slightly decreases through the free surface. In the section between the maximum scour depth to the crest of dune, the $\sqrt{\overline{u'^2}}$ distribution shows a uniform profile. As explained in the previous paragraph, the $\sqrt{\overline{v'^2}}$ distribution in the whole scoured zone section showed smaller values than those of $\sqrt{\overline{u'^2}}$.

7. CONCLUSIONS

A hybrid numerical–mathematical model has been developed for simulating the temporal evolution of local scour and flow patterns downstream of hydraulic structures. The hybrid model contains a mathematical and a numerical module. The mathematical module solves a partial differential equation, which gives the instantaneous shape of scour profile and the numerical module simulates the internal flow characteristics of turbulent flow over and around the scoured zone using k–ε turbulence model. The two modules communicate with each other through a quasi-steady hydrodynamic time-stepping mechanism at the computational program level. The proposed model has been validated by the experimental results of a most recent previous work. The results showed that the proposed hybrid model could predict the local scour and flow patterns downstream of a sill followed by a rigid apron, in strictly good agreement with the experimental results. The specific gain from this study is the potential of a new hybrid technique in modelling local scour and hydrodynamic change around hydraulic structures subjected to turbulent flow.

ACKNOWLEDGEMENTS

The authors wish to thank Prof. Dr Claudio Adduce for her invaluable experimental test results. The financial support of Scientific Research Projects Governing Unit of Gaziantep University is acknowledged by the authors.

DOI: 10.1002/fld

REFERENCES

1. Gunal M, Guven A. Prediction of flow patterns in scoured zone. *Canadian Journal of Civil Engineering* 2006; **33**(1):41–48.
2. Salehi-Neyshabouri AA, Barron RM, Da Silva FAM. Numerical simulation of scour by a wall jet. *Water Engineering Research* 2001; **2**(3):179–185.
3. Zaghloul NA, McCorquodale JA. Stable numerical model for local scour. *Journal of Hydraulic Research* 1975; **13**(4):425–444.
4. Guohou J, Peisheng G. Mathematical model of river bed scouring downstream of stilling basin. *Journal of Hydraulic Engineering* 1988; **114**(4):9–16.
5. Ushijima B, Shimitzu T, Sakasi A, Takizawa Y. Prediction method for local scour by warmed cooling water jets. *Journal of Hydraulic Engineering* 1992; **118**(8):1164–1183.
6. Ushijima S. Arbitrary Lagrangian–Eulerian numerical prediction for local scour caused by turbulent flows. *Journal of Computational Physics* 1996; **125**:71–82.
7. Hoffmans GJCM, Booij R. Two dimensional mathematical modeling of local scour holes. *Journal of Hydraulic Research* 1993; **31**(5):615–634.
8. Van Rijn LC. Mathematical modelling of morphological processes in the case of suspended sediment transport. *Ph.D. Thesis*, Department of Fluid Mechanics, Delft University of Technology, Delft, Netherlands, 1987.
9. Olsen NRB, Melaaen MC. Three-dimensional calculation of scour around a cylinder. *Journal of Hydraulic Engineering* 1993; **119**(9):1048–1053.
10. Hogg AJ, Huppert HE, Dade WB. Erosion by planar turbulent wall jets. *Journal of Fluid Mechanics* 1997; **338**:317–340.
11. Olsen NRB, Kjellesvig HM. Three-dimensional numerical flow modelling for estimation of maximum local scour depth. *Journal of Hydraulic Research* 1998; **36**(4):579–590.
12. Hoffmans GJCM. Jet scour in equilibrium phase. *Journal of Hydraulic Engineering* 1998; **124**(4):430–437.
13. Garcia-Martinez R, Saavedra I, De Power BF, Valera E. A two-dimensional computational model to simulate suspended sediment transport and bed changes. *Journal of Hydraulic Research* 1999; **37**:327–344.
14. Karim OA, Ali KHM. Prediction of flow patterns in local scour caused by turbulent water jets. *Journal of Hydraulic Research* 2000; **38**(4):279–287.
15. Jia Y, Kitamura T, Wang SSY. Simulation of scour process in plunging pool of loose bed-material. *Journal of Hydraulic Engineering* 2001; **127**(3):219–229.
16. Salehi-Neyshaboury AA, Da Silva AMF, Barron R. Numerical simulation of scour by a free falling jet. *Journal of Hydraulic Research* 2003; **41**(5):533–539.
17. Soulis JV. A fully coupled numerical technique for 2D bed morphology calculations. *International Journal for Numerical Methods in Fluids* 2002; **38**(1):71–98.
18. Adduce C, Sciortino G. Scour due to a horizontal jet: numerical and experimental investigation. *Journal of Hydraulic Research* 2006; **44**(5):663–673.
19. Adduce C. Local scour downstream of a turbulent jet. *Ph.D. Thesis*, Department of Civil Engineering, University of Roma Tre, Italy, 2004.
20. Launder BE, Morse A, Rodi W, Spalding DB. A comparison of performance of six turbulence models. *Proceedings of NASA Conference on Free Shear Flows*, Langley, VA, U.S.A., 1972.
21. Patankar SV. *Numerical Heat Transfer and Fluid Flow*. McGraw-Hill Book Company: New York, 1980.
22. Rajaratnam N, Berry S. Erosion by circular turbulent wall jets. *Journal of Hydraulic Research* 1977; **15**(3): 277–289.
23. Long D, Steffler PM, Rajaratnam N. A numerical study of submerged hydraulic jumps. *Journal of Hydraulic Research* 1991; **29**(3):293–308.
24. Launder BE, Spalding DB. The numerical computation of turbulent flows. *Computational Methods in Applied Mechanics and Engineering* 1974; **3**:269–289.
25. Benim AC, Zinser W. Investigation into the finite element analysis of confined turbulent flows using a k–e model of turbulence. *Computer Methods in Applied Mechanics and Engineering* 1985; **51**:507–523.
26. Patankar SV, Spalding DB. A calculation procedure for heat, mass and momentum transfer in three-dimensional parabolic flows. *International Journal of Heat and Mass Transfer* 1972; **15**:1787–1816.
27. Meyer-Peter E, Mueller R. Formulas for bed-load transport. *Proceedings of the 3rd Conference of International Association of Hydraulic Research* (*IAHR*), Stockholm, Sweden, 1948; 39–64.
28. Garcia R, Kahawita RA. Numerical solution of the St. Venant equations with the Mac-Cormack finite difference scheme. *International Journal for Numerical Methods in Fluids* 1995; **6**:259–274.

DOI: 10.1002/fld

29. Guven A. Local scour beneath turbulent jets. *M.Sc. Thesis*, Department of Civil Engineering, University of Gaziantep, Gaziantep, Turkey, 2003.
30. Rajaratnam N. *Turbulent Jets*. Elsevier Scientific Publishing Company: Amsterdam, 1976.
31. Glauert MB. The wall jet. *Journal of Fluid Mechanics* 1956; **1**(6):625–643.
32. Schwarz WH, Cosart WP. The two-dimensional wall-jet. *Journal of Fluid Mechanics* 1961; **10**:481–495.
33. Liriano SL, Day RA, White WR. Scour at culvert outlets as influenced by the turbulent flow structure. *Journal of Hydraulic Research* 2002; **40**(3):367–376.

DOI: 10.1002/fld